Exceptional Air Mass Transport and Dynamical Drivers of an Extreme Wintertime Arctic Warm Event

Hanin Binder, Maxi Boettcher, Christian M. Grams, Hanna Joos, Stephan Pfahl, Heini Wernli

AGU PUBLICATIONS

Geophysical Research Letters

RESEARCH LETTER
10.1002/2017GL075841

Key Points:
- A complex chain of extraordinary dynamical and physical processes resulted in an extreme wintertime Arctic warm event
- The warm air came from three different regions and experienced fundamentally different temperature evolutions before arriving in the Arctic
- Latent heating in ascending airstreams contributed to the setup of an unusual weather pattern that allowed the warm air to reach the Arctic

Supporting Information:
- Supporting Information S1
- Movie S3
- Movie S2
- Movie S1

Correspondence to:
H. Binder,
hanin.binder@env.ethz.ch

Citation:
Binder, H., Boettcher, M., Grams, C. M., Joos, H., Pfahl, S., & Wernli, H. (2017). Exceptional air mass transport and dynamical drivers of an extreme wintertime Arctic warm event. *Geophysical Research Letters*, *44*, 12,028–12,036. https://doi.org/10.1002/2017GL075841

Received 2 OCT 2017
Accepted 31 OCT 2017
Accepted article online 10 NOV 2017
Published online 11 DEC 2017

Exceptional Air Mass Transport and Dynamical Drivers of an Extreme Wintertime Arctic Warm Event

Hanin Binder[1,2], Maxi Boettcher[1], Christian M. Grams[1,3], Hanna Joos[1], Stephan Pfahl[1], and Heini Wernli[1]

[1]Institute for Atmospheric and Climate Science, ETH Zurich, Zurich, Switzerland, [2]Now at Laboratoire de Météorologie Dynamique/IPSL, École Normale Supérieure, Paris, France, [3]Now at Institute of Meteorology and Climate Research (IMK-TRO), Karlsruhe Institute of Technology, Karlsruhe, Germany

Abstract At the turn of the years 2015/2016, maximum surface temperature in the Arctic reached record-high values, exceeding the melting point, which led to a strong reduction of the Arctic sea ice extent in the middle of the cold season. Here we show, using a Lagrangian method, that a combination of very different airstreams contributed to this event: (i) warm low-level air of subtropical origin, (ii) initially cold low-level air of polar origin heated by surface fluxes, and (iii) strongly descending air heated by adiabatic compression. The poleward transport of these warm airstreams occurred along an intense low-level jet between a series of cyclones and a quasi-stationary anticyclone. The complex 3-D configuration that enabled this transport was facilitated by continuous warm conveyor belt ascent into the upper part of the anticyclone. This study emphasizes the combined role of multiple transport processes and transient synoptic-scale dynamics for establishing an extreme Arctic warm event.

1. Introduction

In recent decades, the increase in surface air temperatures has been much stronger in the Arctic compared to the global average—a process referred to as Arctic amplification (Serreze & Barry, 2011; Serreze & Francis, 2006; Stocker et al., 2013). As a consequence, Arctic sea ice cover and land ice concentrations have diminished significantly since the beginning of the modern satellite period in 1979 (Mernild et al., 2011; Simmonds, 2015; Stroeve et al., 2007). Possible reasons for this enhanced Arctic warming are the positive albedo feedback associated with melting snow and ice (Arrhenius, 1896; Screen & Simmonds, 2010), different radiative feedbacks at low and high latitudes (Pithan & Mauritsen, 2014), changes in Arctic cloud cover and atmospheric water vapor (Graversen & Wang, 2009; Winton, 2006), changes in atmospheric circulation patterns (Willett, 1950), and an increased poleward transport of heat and moisture (Graversen et al., 2008; Rinke et al., 2017; Woods & Caballero, 2016).

Superimposed on the long-term Arctic warming and ice reduction were several short-term episodes with particularly high temperatures and enhanced melting, for instance, the record Arctic sea ice decline in summer 2007 (Graversen et al., 2011), an extreme heat and melt event over Greenland in July 2012 (Nghiem et al., 2012), and a period of rapid sea ice reduction in the East Siberian Sea in August 2014 (Tjernström et al., 2015). During all these episodes the poleward advection of warm and moist air (Bonne et al., 2015; Graversen et al., 2011; Neff et al., 2014; Sedlar & Devasthale, 2012; Tjernström et al., 2015), and radiative effects associated with the formation of low-level liquid clouds and fog (Bennartz et al., 2013; Graversen et al., 2011; Tjernström et al., 2015), contributed essentially to the high Arctic temperatures and strong ice melting. The primary role of advection for warm extremes in the Arctic is in contrast to the processes leading to warm extremes in the midlatitudes. There, warm extremes generally result from strong adiabatic warming in the colocated blocking anticyclones (Pfahl & Wernli, 2012), as well as diabatic heating from enhanced incoming solar radiation and surface sensible heat fluxes (Bieli et al., 2015).

In addition to the above mentioned Arctic summertime heat episodes, extreme warm events in winter can also substantially impact Arctic sea ice conditions. In late December 2015 and early January 2016 such a major wintertime Arctic warm event occurred (Boisvert et al., 2016; Cullather et al., 2016; Kim et al., 2017; Moore, 2016), which contributed to making 2015/2016 the warmest Arctic winter in the observational record (Cullather et al., 2016). As we will show, the extreme event was the result of a very unusual large-scale flow configuration

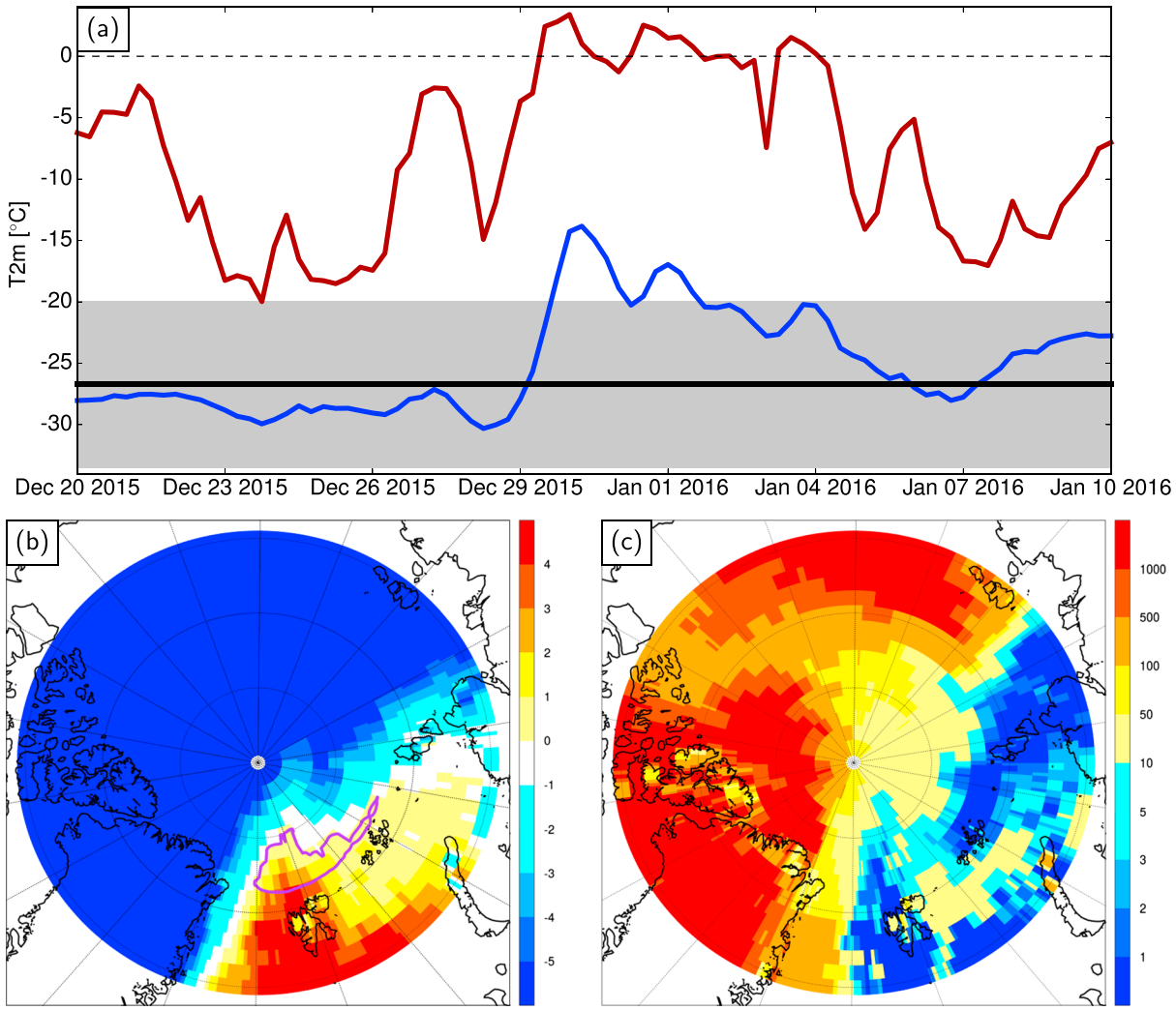

Figure 1. Illustration of the Arctic warm event and its extremeness. (a) Temporal evolution of the domain maximum (red) and mean (blue) T2m (°C) between 20 December 2015 and 10 January 2016 at latitudes ≥82°N and between 120°W and 120°E, derived from operational analyses. Also shown are the domain mean December–February 1979–2014 climatological mean T2m (black), and the corresponding ±1 standard deviation envelope (grey) from ERA-Interim reanalysis data. (b) Maximum T2m (°C) between 00 UTC 30 December 2015 and 18 UTC 4 January 2016 from operational analyses, with the purple contour highlighting the regions ≥82°N with maximum T2m ≥ 0°C. (c) Rank of maximum T2m shown in Figure 1b among all 6-hourly values in winter 1979–2014 in the ERA-Interim reanalyses (consisting of a total of 13,232 values).

in early winter 2015/2016 that came along with overall anomalously warm conditions in Europe (National Oceanic and Atmospheric Administration, 2016) and other regional extremes, for example, flooding in the UK (Marsh et al., 2016). In this study, we focus on the Arctic. At the North Pole, buoys measured maximum surface temperatures of −0.8°C on 30 December (Moore, 2016), and at the Svalbard airport station values of 8.7°C were observed, the warmest temperatures ever recorded at that station between November and April (The Norwegian Meteorological Institute, 2016). According to operational analyses from the European Centre for Medium-Range Weather Forecasts (ECMWF), the maximum 2 m temperature (T2m) north of 82°N reached values larger than 0°C during three short episodes between 29 December 2015 and 4 January 2016—almost 30 K above the winter climatological mean in this region (Figure 1a). They occurred in the Eurasian Arctic sector in the region around Svalbard and over the Kara Sea (purple contour in Figure 1b) and were the highest winter values since 1979 (Figure 1c). The warm event led to a thinning of the sea ice by more than 30 cm in the Barents and Kara Seas, and contributed to the record low Northern Hemisphere sea ice extent observed in January and February 2016 (National Snow and Ice Data Center, 2016).

Media reports (Gosden, 2015; Samenow, 2015) and previous studies (Boisvert et al., 2016; Cullather et al., 2016; Kim et al., 2017) explained the onset of the extreme event by the poleward advection of heat and moisture

by storm "Frank," which moved over Iceland on 30 December 2015 as one of the strongest North Atlantic storms on record (Kim et al., 2017). According to Kim et al. (2017), the subsequent formation of a blocking anticyclone over Scandinavia and northwestern Russia, and strong downward longwave radiation associated with the surface warm anomaly, contributed to sustaining the high temperatures in the Arctic. In contrast, Moore (2016) attributed the warming to a perturbed polar vortex and an Arctic cyclone that advected warm and moist air from the nearby Nordic Seas. These diverging interpretations illustrate that the processes leading to this exceptional extreme event are not yet fully explained.

Individual weather events can be important for establishing anomalous seasonal flow patterns, and thereby they account for interannual flow variability (Davies, 2015; Wernli & Papritz, 2017). Thus, understanding the processes that resulted in the high surface temperatures in the Arctic at the turn of the years 2015/2016 is important not only because of the extreme character of the event but also because it helps in gaining insight into factors that contribute to interannual variability of Arctic temperature and ice concentrations, which are superimposed onto the long-term Arctic warming and ice decline. In this study we aim to clarify the origin of the air masses that led to the extreme event and to unveil the meteorological processes responsible for their poleward transport. Moreover, to place the results in a climatological context, the identified source regions, transport processes and synoptic features are compared with reanalysis data from the previous 36 winters.

2. Data and Methods

2.1. Data

The study is based on operational high-resolution analysis data from the ECMWF Integrated Forecast System (IFS), available every 6 h and interpolated to a regular grid with 0.5° horizontal grid spacing. For the considered time period at the turn of the years 2015/2016, these analyses were produced with the IFS model version Cycle 41r1 with a resolution of T1279L137. For the climatological investigations, 6-hourly ERA-Interim reanalyses from ECMWF (Dee et al., 2011; Simmons et al., 2007) are used for the winters 1979–2014 (which refers to the months December–February, starting in January 1979 and ending in February 2015), available at T255L60 and interpolated to a 1° horizontal grid.

2.2. Backward Trajectory Calculations

To reconstruct the history of the air that contributed to the extreme warm event, three-dimensional kinematic backward trajectories are calculated with the Lagrangian Analysis Tool LAGRANTO (Sprenger & Wernli, 2015; Wernli & Davies, 1997) from ≥82°N and between 120°W and 120°E, every 6 h between 00 UTC 27 December 2015 and 18 UTC 4 January 2016. The trajectories are initialized on a regular grid with 40 km horizontal spacing and vertically at five pressure levels located 10, 30, 50, 70, and 90 hPa above the surface, at all grid points where T2m is ≥0°C, and calculated 10 days backward in time. The temperature threshold of 0°C emphasizes the regions where the impact of the warm plumes on the Arctic sea ice was highest, and the restriction to latitudes ≥82°N excludes Svalbard, where Foehn effects likely contributed to the particularly high temperatures. The horizontal position, pressure, temperature (T), and potential temperature (θ) are traced along the trajectory path. To relate temperature changes of the air parcels to adiabatic and diabatic processes, for each backward trajectory the maximum absolute difference between the T value at the starting point in the Arctic and the previous maximum or minimum value along the trajectory path, ΔT, is calculated, and analogously for θ. Trajectories with positive (negative) ΔT experienced an overall temperature increase (decrease) before contributing to the high temperatures in the Arctic, and analogously, trajectories with positive (negative) values of $\Delta\theta$ primarily experienced diabatic heating (cooling). This characterization will be very useful to identify three categories of airstreams with strongly differing properties.

For the climatological investigation, the trajectory calculations are repeated with ERA-Interim for the winter period 1979–2014. The setup of the calculations is the same as for the warm event, except that the horizontal resolution of the starting grid is 80 km instead of 40 km. Furthermore, in contrast to the event the backward trajectories from the Arctic region are started from all grid points irrespective of the T2m value, in order to assess typical source regions and transport processes of air masses reaching the Arctic under "normal" conditions and during previous warm events.

3. Results

3.1. Origin of the Warm Air Masses

Figure 2a shows for all trajectories contributing to the Arctic warm event the maximum absolute change in temperature, ΔT, and potential temperature, $\Delta\theta$, relative to their arrival in the Arctic (see section 2.2).

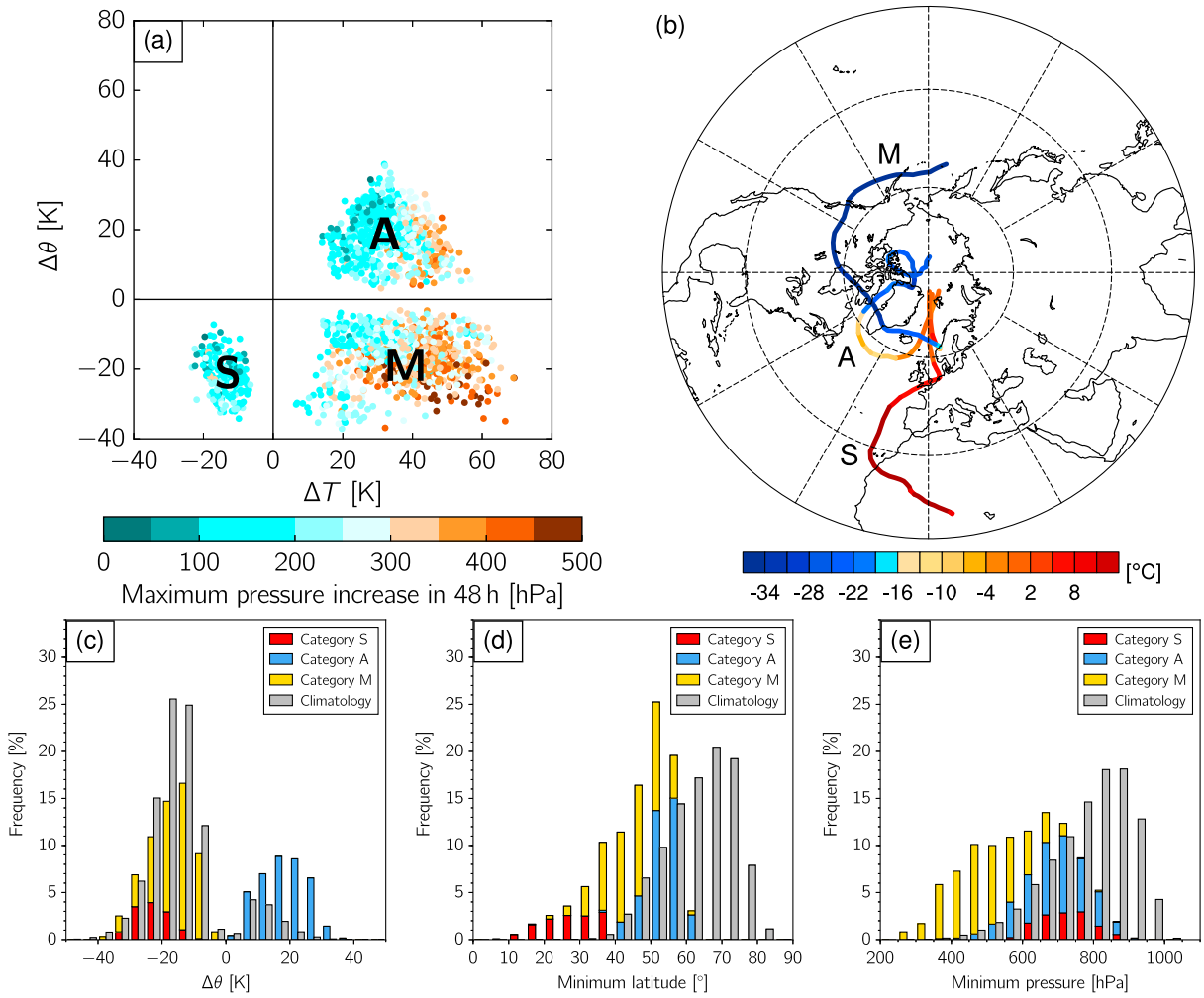

Figure 2. History of the air masses contributing to the Arctic warm event. (a) Phase-space diagram illustrating for all trajectories the maximum absolute change in temperature (ΔT, K) and potential temperature ($\Delta\theta$, K), relative to the time when the trajectories arrived in the Arctic, together with the maximum positive change in pressure (i.e., descent) of all 48 h intervals along the trajectories (shading, hPa). (b) Evolution of temperature (°C) along three backward trajectories from the warm event that represent the main characteristics of air mass categories S, A, and M. Histogram showing the relative occurrence frequency of (c) $\Delta\theta$ (bin width = 5 K), (d) minimum latitude (bin width = 5°), and (e) minimum pressure (bin width = 50 hPa) along the trajectories contributing to the Arctic warm event (sum of red, blue, and yellow bars), derived from operational analyses. The stacked colors indicate the division of the histogram into categories S (red), A (blue), and M (yellow). For comparison, a separate histogram (grey) shows the corresponding occurrence frequencies along all ERA-Interim backward trajectories from the Arctic during December–February 1979–2014.

The phase-space diagram reveals three clearly separated categories: air parcels in category S experienced a dominant temperature decrease and diabatic cooling prior to their arrival in the Arctic (negative ΔT and $\Delta\theta$, 12% of all trajectories), air parcels in category A experienced a temperature increase and diabatic heating (positive ΔT and $\Delta\theta$, 37% of all trajectories), and air parcels in category M experienced a temperature increase and diabatic cooling (positive ΔT and negative $\Delta\theta$, 51% of all trajectories).

The position of the air parcels 10 days before arriving in the Arctic reveals that the three categories can broadly be related to three different source regions (Figure 2b and Figure S2 in the supporting information): the subtropical lower troposphere over the Sahara and the western Mediterranean (category S; Figures S2a and S2d), the Arctic lower troposphere (category A; Figures S2b and S2e), and a broader region at middle to high latitudes in the middle and upper troposphere (category M; Figures S2c and S2f). The subtropical air parcels in category S were initially relatively warm (typical temperature values greater than 5°C and maxima above 20°C; Figure S2a). They were continuously cooled during their subsequent poleward low-level transport (representative trajectory "S" in Figure 2b; see also Movie S1 for the pathways and temperature evolution of all category S air parcels). In contrast, the air parcels originating at middle to high latitudes at low (category A)

or upper levels (category M) were initially extremely cold (typical temperatures of less than −20°C and minima below −60°C; Figures S2b and S2c). These trajectories subsequently experienced a strong warming (see representative trajectories "A" and "M" in Figure 2b and Movies S2 and S3). In spite of the very different origin and temperature evolution of the air masses in the three categories, they all arrived in the Arctic with roughly the same, anomalously high temperature.

The air parcels in Figure 2a are colored according to their maximum pressure increase (i.e., descent) over all 48 h time intervals along the trajectory path. The majority of the air parcels in categories S and A remained close to the surface during the entire 10 day period. In category S, the negative changes in ΔT and $\Delta\theta$ resulted from diabatic cooling of the warm subtropical air masses by air-sea heat fluxes when they moved over colder surfaces during their poleward transport (Figure S3). However, comparison with all trajectories that reached the low-level Arctic during the previous 36 winters (see section 2.2) shows that this diabatic cooling of the category S air parcels was relatively weak and in the same range as the climatological values (compare red and grey bars in Figure 2c), such that they still reached the Arctic with temperatures above the melting point. Such a strong meridional transport of subtropical air into low-level Arctic regions is extremely rare (Figure 2d): While during the event almost one quarter of all trajectories reaching the Arctic originated from latitudes south of 40°N (colored bars in Figure 2d, with the main contribution from the red bars associated with category S), this was the case for only 0.7% of the trajectories during the previous 36 winters (grey bars). Note that in Figures 2c–2e the histograms for the event are derived from operational analyses, while the climatology is derived from ERA-Interim reanalyses. However, the ERA-Interim-based histograms for the event agree with those based on operational analyses (Figure S5).

The positive changes in ΔT and $\Delta\theta$ in category A (see again Figure 2a) are due to diabatic heating of the cold, dry polar air masses by intense surface fluxes when they moved over warmer ocean water during a cold air outbreak (Figure S4; see also Papritz & Spengler, 2017). This diabatic heating was unusually strong, as evident when comparing the blue bars in Figure 2c with the climatological frequency distribution of $\Delta\theta$ (grey bars in Figure 2c).

In contrast to the other categories, the air parcels in category M typically experienced a strong descent of up to 500 hPa in 48 h (Figure 2a), which went along with a very pronounced adiabatic warming (see also Bieli et al., 2015). The weaker negative changes in θ (Figure 2a) can most likely be explained by a concomitant longwave radiative cooling during the descent (Cau et al., 2007; Raveh-Rubin, 2017). The strong descent and adiabatic warming were also extremely unusual: One quarter of all trajectories that contributed to the warm event descended from the upper troposphere (minimum pressure <500 hPa, colored bars in Figure 2e, with the main contribution from the yellow bars associated with category M) compared to only 1.7% in the climatology (grey bars in Figure 2e). Almost 8% of the event-related trajectories experienced a temperature increase of more than 50 K (Figures 2a and S6, again with the main contribution from category M), while this was only the case for 0.03% of the trajectories during the previous 36 winters (Figure S6).

From more than 18 million trajectories calculated from low-level Arctic regions (i.e., from latitudes ≥82°N and between 120°W and 120°E) during the winters 1979–2014, only 0.016% arrived there with T2m ≥ 0°C, corroborating the exceptional nature of the warm event discussed in this study. As a side remark, note that in 12 out of the 36 winters such an extreme Arctic warm event occurred, with the earliest event taking place in winter 1984/1985, and the four most recent events between winters 2009/2010 and 2014/2015 (not shown). The trajectories of this small climatological fraction and those associated with the warm event in 2015/2016 are similar in terms of ΔT, $\Delta\theta$, minimum latitude, and minimum pressure (Figure S7). Consistent with previous findings (Moore, 2016), this suggests that similar dynamical and physical processes played a role during different Arctic warm events. However, despite the similar distribution, the warm event in late December 2015 and early January 2016 clearly stands out from the other warm events in terms of meridional transport from subtropical regions in category S (compare nontransparent and semitransparent red bars in Figure S7c), diabatic heating of originally cold air masses by surface fluxes in category A (compare nontransparent and semitransparent blue bars in Figure S7b), and adiabatic warming of descending air in category M (compare nontransparent and semitransparent yellow bars in Figures S7a and S7d).

3.2. Unusual Weather Evolution

After investigating the history of the air that contributed to the Arctic warm event, and revealing three types of airstreams with fundamentally different origin, temperature evolution, and experienced physical processes,

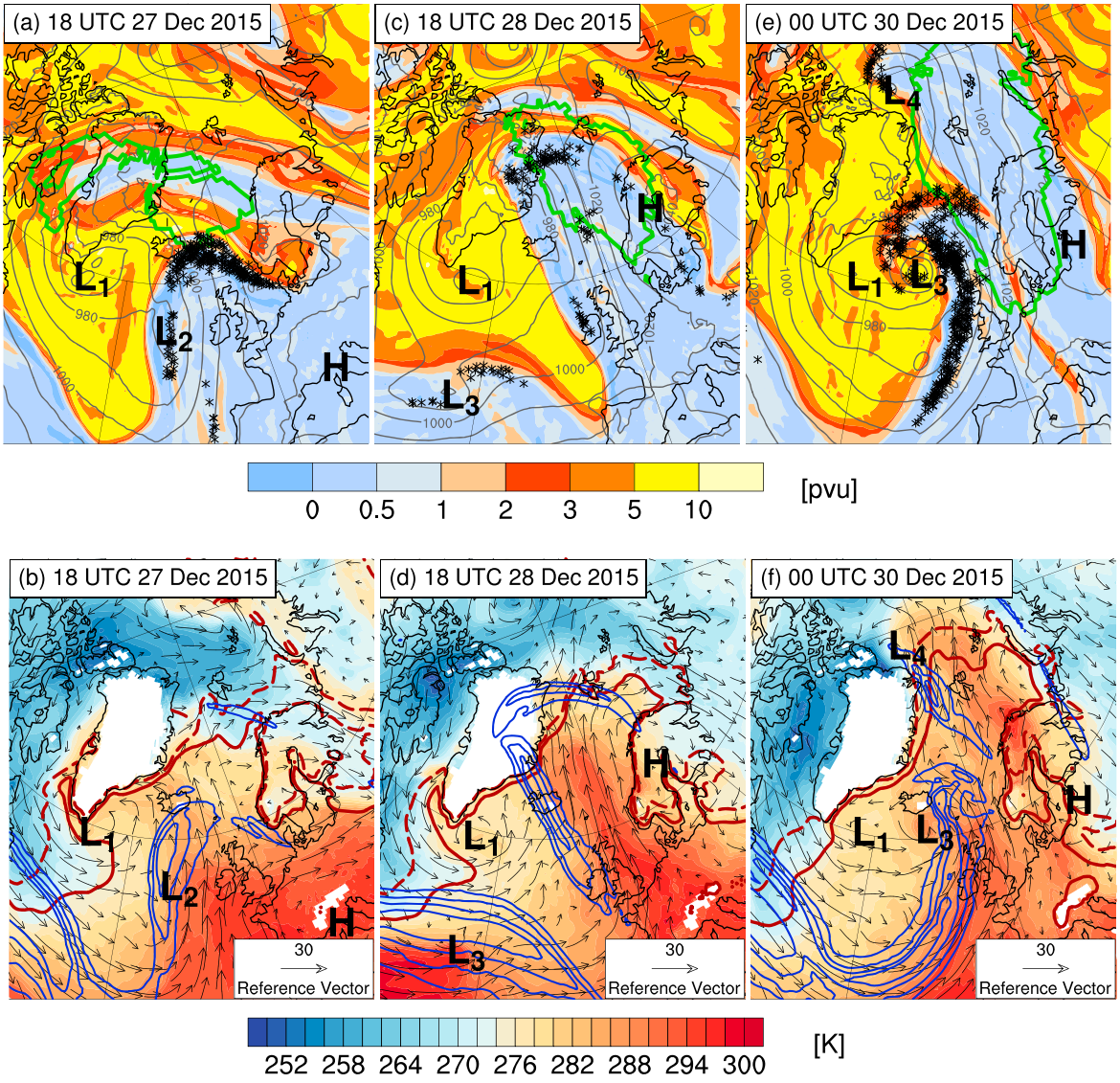

Figure 3. Synoptic situation prior to and at the beginning of the Arctic warm event, at (a, b) 18 UTC 27 December 2015, (c, d) 18 UTC 28 December, and (e, f) 00 UTC 30 December. Top panels: PV on 310 K (pvu, shading), SLP (hPa, black contours every 10 hPa), outline of identified blockings (green contours), and every 10th WCB trajectory intersection with the layer 310 K ±5 K (black asterisks). Bottom panels: Potential temperature (K, shading) and wind vectors (m s^{-1}) at 850 hPa, wind speed at 250 hPa (blue contours for 50, 60, 70, and 80 m s^{-1}), and T2m (red solid and dashed contours for 0 and −5°C, respectively). The labels mark the positions of surface cyclones ("L_1"–"L_4"; the strongly intensifying cyclone "Frank" is denoted as "L_3") and anticyclones ("H").

we now explore the meteorological setting that enabled their progression into the Arctic. During the days preceding the warm event, several cyclones developed close to an upper-level trough over the central North Atlantic (labels "L_1" and "L_2" in Figures 3a and 3b). Ahead of the cyclones, warm and moist airstreams denoted as warm conveyor belts (WCBs; e.g., Browning, 1971; Wernli & Davies, 1997) ascended from the surface warm sector into the upper troposphere, as indicated by the black asterisks in Figure 3a (see Madonna et al., 2014, for details on the WCB identification). Such a strong WCB ascent is always associated with intense latent heating and the formation of clouds and precipitation (Browning, 1990). The cloud diabatic processes lead to potential vorticity (PV) modifications (Hoskins et al., 1985), whereby PV is produced in the early phase of the WCB ascent at low levels and destroyed in the WCB outflow at upper levels (Binder et al., 2016; Madonna et al., 2014; Wernli & Davies, 1997). Thus, as a net effect the WCB transports low-PV air into the tropopause region, which is illustrated by the WCB intersection positions with the 310 K isentropic surface in Figure 3a (i.e., the black asterisks). As evident by the location of the WCB intersections at the poleward edge of the upper-level ridge

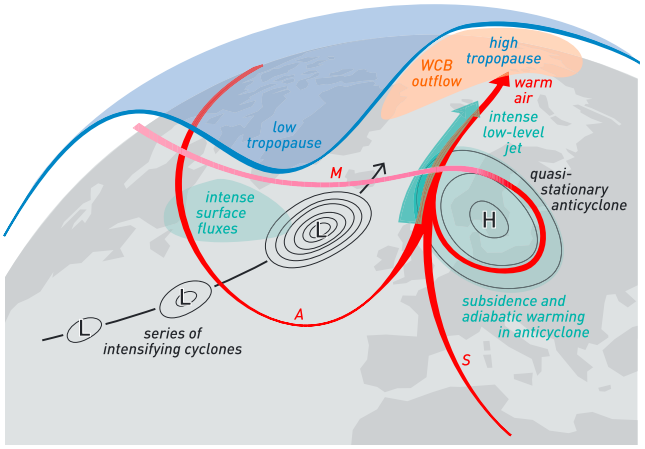

Figure 4. Schematic illustration of the unusual processes that led to the Arctic warm event. A series of North Atlantic cyclones ("L") developed close to an upper-level trough (low tropopause; blue). The strong WCB ascent ahead of the surface cyclones contributed to the far poleward extension of the upper-level ridge (high tropopause north of Svalbard coinciding with the WCB outflow), and the formation of a quasi-stationary surface anticyclone over Scandinavia ("H"). Between the North Atlantic cyclones and the anticyclone an intense poleward low-level jet developed (green arrow), which transported the warm air masses S, A and M (red arrows) into the Arctic. The warm air masses came from three different source regions and were associated with fundamentally different processes: (S) warm low-level air originating in the subtropics, which was rapidly transported northward, (A) initially cold low-level air originating in polar regions, which was heated by intense surface heat fluxes (green patch over the western North Atlantic), and (M) initially cold midlatitude air originating in the upper troposphere, which was heated adiabatically (green patch over Scandinavia) as it descended in the Scandinavian anticyclone. The color of airstream M illustrates its height, with pink indicating upper-level and red low-level air. The figure has been designed by Sandro Bösch (ETH Zurich).

between Iceland and Scandinavia, this upward transport of low-PV air in the WCB contributed to the diabatic amplification of the ridge (see also Grams et al., 2011 and Pfahl et al., 2015).

Along the western side of the ridge a poleward upper-level jet developed (blue contours in Figure 3b), and at the surface, a pronounced poleward low-level jet (black arrows in Figure 3b) established between the Icelandic lows "L_1" and "L_2" and the high-pressure system "H" over Europe (Figures 3a and 3b). Note that at this time cyclone "Frank" was located near Newfoundland and still very weak (not shown). While this exceptional storm contributed to the maintenance of the unusual synoptic situation (see cyclone marked "L_3" in Figures 3e, 3f, and S8 discussed below), the initiation of the extreme Arctic warm event was linked to a series of other strong cyclones and associated WCBs located over the central North Atlantic prior to the genesis of "Frank." Such a serial occurrence of cyclones is sometimes referred to as "cyclone clustering" (Mailier et al., 2006; Pinto et al., 2014).

During the subsequent days, the upper-level trough over the western North Atlantic and the downstream ridge strongly amplified (Figures 3c and 3e). WCB air masses continued to ascend ahead of the Icelandic cyclones, and the low-PV air in their outflow further enhanced the upper-level ridge. Eventually this led to the formation of a strong, persistent blocking anticyclone (see Croci-Maspoli et al., 2007; Pfahl & Wernli, 2012; Schwierz et al., 2004, for details on the blocking identification) that extended from Central Europe far into the Arctic (green contours in Figures 3c and 3e; see also Pfahl et al., 2015).

This dipolar pattern in the upper troposphere went along with the formation of one of the most intense west-to-east surface pressure gradients and the strongest poleward low-level and upper-level meridional jets between Iceland and Northern Europe in the entire modern reanalysis period (Table S1 in the supporting information and Figures 3d and 3f). The intense low-level jet transported warm air northward (Figures 3b and 3d), resulting in an anomalously far poleward extension of the warm plume (Figure 3f). Beginning at 12 UTC 29 December 2015, this plume led to Arctic surface air temperatures above the melting point (Figures 1a and 3f). The synoptic situation remained similar during the following days, with low-PV air in the WCB outflow maintaining the Arctic block, and continuous poleward warm advection across the persistent west-east SLP gradient (Figures S8–S10; see also detailed synoptic description in Binder, 2016). Interrupted by two short episodes during which the region closest to the pole returned to slightly colder conditions (Figure 1a; the synoptic situation during the second colder phase on 2 January 2016 is shown in Figures S8c and S8d), two additional warm plumes with T2m $\geq$ 0°C reached the Arctic on 31 December 2015 and 3 January 2016 in the warm sector of two Arctic mesocyclones ("L_5" and "L_6" in Figures S8a, S8b, S8e, and S8f).

The rapid horizontal transport of the warm air by the exceptionally strong poleward low-level jet, and the fact that this transport occurred mainly over the relatively warm ocean, explain why the subtropical air in category S still reached the Arctic with temperatures above 0°C. The cold air outbreak responsible for the equatorward advection and strong heating of the Arctic air masses in category A occurred in the cold sector of one of the surface cyclones that contributed to the low pressure over Iceland ("L_1" in Figures 3 and S4). In the warm sector of a subsequent Icelandic cyclone, these air parcels were then again transported into the Arctic along the strong poleward jet. Also, the temperature evolution of the air parcels in category M can be explained by the unusual synoptic situation: The intense high-pressure system that formed over Northern Europe below the upper-level blocking anticyclone ("H" in Figures 3c–3f) resulted in strong subsidence in this region. Thus, the category M air parcels that moved from west to east along the upper-level wave guide descended adiabatically over western Norway, whereby they further enlarged the poleward extending warm pool associated with the approach of airstreams S and A.

4. Conclusions

In this study, we investigated the dynamical and physical mechanisms leading to record high temperatures in the Arctic at the turn of the years 2015/2016. As illustrated schematically in Figure 4, the extreme event was the result of a combination of several very unusual processes: (i) rapid meridional transport of warm subtropical air (airstream S), (ii) intense heating of originally cold polar air by air-sea heat fluxes (airstream A), and (iii) strong adiabatic warming of originally cold upper-tropospheric air (airstream M). The transport of these fundamentally different warm air masses S, A, and M to the North Pole was facilitated by the poleward extension of an intense upper-level blocking anticyclone, which was supported by continuous WCB ascent in association with a series of Icelandic cyclones (Figure 4). The poleward warm advection occurred along an unusually strong low-level jet that formed between the Icelandic cyclones and a quasi-stationary Scandinavian surface anticyclone (Figure 4). Our quantitative Lagrangian analysis showed that it was the complex superposition of diverse synoptic-scale dynamical processes that made this event so extreme–attributing the Arctic warm event to a single process would therefore be an unjustified simplification. In addition to these short-term processes, it is likely that the pronounced long-term warming trend in polar regions also played a role for the extreme amplitude of the event. Attribution studies are needed to quantify the contribution of climate change and Arctic amplification to such extreme events, and their potentially increased occurrence in a future climate.

Acknowledgments
MeteoSwiss and ECMWF are acknowledged for granting access to the ECMWF analysis and reanalysis data. We thank Sandro Bösch (ETH Zurich) for designing the schematic illustration in Figure 4, and Roman Attinger, Marina Dütsch, and Stefan Rüdisühli (ETH Zurich) for technical support. We are also grateful to Joaquim Pinto and an anonymous reviewer for their constructive comments. H. B., M. B., and C. M. G. acknowledge funding from the Swiss National Science Foundation (SNSF) via grants 200020_146834 (H. B.), 200020_165941 (M. B.), and PZ00P2_148177/1 (C. M. G.). The ERA-Interim data used in this study can be accessed from the ECMWF website (https://software.ecmwf.int/wiki/display/WEBAPI/Access+ECMWF+Public+Datasets). The results of the study are available from the authors upon request.

References

Arrhenius, S. (1896). On the influence of carbonic acid in the air upon the temperature of the ground. *Philosophical Magazine and Journal of Science*, *41*, 237–276.

Bennartz, R., Shupe, M. D., Turner, D. D., Walden, V. P., Steffen, K., Cox, C. J., … Pettersen, C. (2013). July 2012 Greenland melt extent enhanced by low-level liquid clouds. *Nature*, *496*, 83–86.

Bieli, M., Pfahl, S., & Wernli, H. (2015). A Lagrangian investigation of hot and cold temperature extremes in Europe. *Quarterly Journal of the Royal Meteorological Society*, *141*, 98–108.

Binder, H. (2016). Warm conveyor belts: Cloud structure and role for cyclone dynamics and extreme events (Ph.D. Thesis), Zurich, ETH Zurich.

Binder, H., Boettcher, M., Joos, H., & Wernli, H. (2016). The role of warm conveyor belts for the intensification of extratropical cyclones in Northern Hemisphere winter. *Journal of the Atmospheric Sciences*, *73*, 3997–4020.

Boisvert, L. N., Petty, A. A., & Stroeve, J. C. (2016). The impact of the extreme winter 2015/16 Arctic cyclone on the Barents–Kara Seas. *Monthly Weather Review*, *144*, 4279–4287.

Bonne, J.-L., Steen-Larsen, H. C., Risi, C., Werner, M., Sodemann, H., Lacour, J.-L., … Masson-Delmotte, V. (2015). The summer 2012 Greenland heat wave: In situ and remote sensing observations of water vapor isotopic composition during an atmospheric river event. *Journal of Geophysical Research: Atmospheres*, *120*, 2970–2989. https://doi.org/10.1002/2014JD022602

Browning, K. A. (1971). Radar measurements of air motion near fronts. *Weather*, *26*, 320–340.

Browning, K. A. (1990). Organization of clouds and precipitation in extratropical cyclones. In C. W. Newton & E. O. Holopainen (Eds.), *Extratropical cyclones: The Erik Palmén memorial volume* (pp. 129–153). Boston, MA: American Meteorological Society.

Cau, P., Methven, J., & Hoskins, B. (2007). Origins of dry air in the tropics and subtropics. *Journal of Climate*, *20*, 2745–2759.

Croci-Maspoli, M., Schwierz, C., & Davies, H. C. (2007). A multifaceted climatology of atmospheric blocking and its recent linear trend. *Journal of Climate*, *20*, 633–649.

Cullather, R. I., Lim, Y.-K., Boisvert, L. N., Brucker, L., Lee, J. N., & Nowicki, S. M. (2016). Analysis of the warmest Arctic winter, 2015–2016. *Geophysical Research Letters*, *43*, 10,808–10,816. https://doi.org/10.1002/2016GL071228

Davies, H. C. (2015). Weather chains during the 2013/2014 winter and their significance for seasonal prediction. *Nature Geoscience*, *8*, 833–837.

Dee, D. P., Uppala, S. M., Simmons, A. J., Berrisford, P., Poli, P., Kobayashi, S., … Vitart, F. (2011). The ERA-Interim reanalysis: configuration and performance of the data assimilation system. *Quarterly Journal of the Royal Meteorological Society*, *137*, 553–597.

Gosden, E. (2015). North Pole temperatures spike "above freezing" as Storm Frank sends warm air north. In *The Telegraph*. London, United Kingdom.

Grams, C. M., Wernli, H., Böttcher, M., Campa, J., Corsmeier, U., Jones, S. C., … Wiegand, L. (2011). The key role of diabatic processes in modifying the upper-tropospheric wave guide: A North Atlantic case-study. *Quarterly Journal of the Royal Meteorological Society*, *137*, 2174–2193.

Graversen, R. G., & Wang, M. (2009). Polar amplification in a coupled climate model with locked albedo. *Climate Dynamics*, *33*, 629–643.

Graversen, R. G., Mauritsen, T., Drijfhout, S., Tjernström, M., & Mårtensson, S. (2011). Warm winds from the Pacific caused extensive Arctic sea-ice melt in summer 2007. *Climate Dynamics*, *36*, 2103–2112.

Graversen, R. G., Mauritsen, T., Tjernström, M., Källén, E., & Svensson, G. (2008). Vertical structure of recent Arctic warming. *Nature*, *451*, 53–56.

Hoskins, B. J., McIntyre, M. E., & Robertson, A. W. (1985). On the use and significance of isentropic potential vorticity maps. *Quarterly Journal of the Royal Meteorological Society*, *111*, 877–946.

Kim, B.-M., Hong, J.-Y., Jun, S.-Y., Zhang, X., Kwon, H., Kim, S.-J., … Kim, H.-K. (2017). Major cause of unprecedented Arctic warming in January 2016: Critical role of an Atlantic windstorm. *Scientific Reports*, *7*, 40051.

Madonna, E., Wernli, H., Joos, H., & Martius, O. (2014). Warm conveyor belts in the ERA-Interim dataset (1979–2010). Part I: Climatology and potential vorticity evolution. *Journal of Climate*, *27*, 3–26.

Mailier, P. J., Stephenson, D. B., Ferro, C. A., & Hodges, K. I. (2006). Serial clustering of extratropical cyclones. *Monthly Weather Review*, *134*, 2224–2240.

Marsh, T. J., Kirby, C., Muchan, K., Barker, L., Henderson, E., & Hannaford, J. (2016). *The winter floods of 2015/2016 in the UK—A review*. Wallingford, UK: Centre for Ecology and Hydrology.

Mernild, S. H., Mote, T. L., & Liston, G. E. (2011). Greenland ice sheet surface melt extent and trends: 1960–2010. *Journal of Glaciology*, *57*, 621–628.
Moore, G. W. K. (2016). The December 2015 North Pole warming event and the increasing occurrence of such events. *Scientific Reports*, *6*, 39084.
National Oceanic and Atmospheric Administration (2016). Land and ocean temperature percentiles Dec 2015. Retrieved from https://www.ncdc.noaa.gov/sotc/service/global/map-percentile-mntp/201512.gif
National Snow and Ice Data Center (2016). March ends a most interesting winter. Retrieved from https://nsidc.org/arcticseaicenews/2016/04/march-ends-a-most-interesting-winter
Neff, W., Compo, G. P., Ralph, F. M., & Shupe, M. D. (2014). Continental heat anomalies and the extreme melting of the Greenland ice surface in 2012 and 1889. *Journal of Geophysical Research: Atmospheres*, *119*, 6520–6536. https://doi.org/10.1002/2014JD021470
Nghiem, S. V., Hall, D. K., Mote, T. L., Tedesco, M., Albert, M. R., Keegan, K., … Neumann, G. (2012). The extreme melt across the Greenland ice sheet in 2012. *Geophysical Research Letters*, *39*, L20502. https://doi.org/10.1029/2012GL053611
Papritz, L., & Spengler, T. (2017). A Lagrangian climatology of wintertime cold air outbreaks in the Irminger and Nordic Seas and their role in shaping air–sea heat fluxes. *Journal of Climate*, *30*, 2717–2737.
Pfahl, S., & Wernli, H. (2012). Quantifying the relevance of atmospheric blocking for co-located temperature extremes in the Northern Hemisphere on (sub-)daily time scales. *Geophysical Research Letters*, *39*, L12807. https://doi.org/10.1029/2012GL052261
Pfahl, S., Schwierz, C., Croci-Maspoli, M., Grams, C. M., & Wernli, H. (2015). Importance of latent heat release in ascending air streams for atmospheric blocking. *Nature Geoscience*, *8*, 610–614.
Pinto, J. G., Gómara, I., Masato, G., Dacre, H. F., Woollings, T., & Caballero, R. (2014). Large-scale dynamics associated with clustering of extratropical cyclones affecting Western Europe. *Journal of Geophysical Research: Atmospheres*, *119*, 13,704–13,719. https://doi.org/10.1002/2014JD022305
Pithan, F., & Mauritsen, T. (2014). Arctic amplification dominated by temperature feedbacks in contemporary climate models. *Nature Geoscience*, *7*, 181–184.
Raveh-Rubin, S. (2017). Dry intrusions: Lagrangian climatology and dynamical impact on the planetary boundary layer. *Journal of Climate*, *30*, 6661–6682.
Rinke, A., Maturilli, M., Graham, R. M., Matthes, H., Handorf, D., Cohen, L., … Moore, J. C. (2017). Extreme cyclone events in the Arctic: Wintertime variability and trends. *Environmental Research Letters*, *12*, 094006.
Samenow, J. (2015). Freak storm in North Atlantic to lash UK, may push temperatures over 50 degrees above normal at North Pole. In *The Washington Post*. Washington, DC, United States.
Schwierz, C., Croci-Maspoli, M., & Davies, H. C. (2004). Perspicacious indicators of atmospheric blocking. *Geophysical Research Letters*, *31*, L06125. https://doi.org/10.1029/2003GL019341
Screen, J. A., & Simmonds, I. (2010). The central role of diminishing sea ice in recent Arctic temperature amplification. *Nature*, *464*, 1334–1337.
Sedlar, J., & Devasthale, A. (2012). Clear-sky thermodynamic and radiative anomalies over a sea ice sensitive region of the Arctic. *Journal of Geophysical Research*, *117*, D19111. https://doi.org/10.1029/2012JD017754
Serreze, M. C., & Barry, R. G. (2011). Processes and impacts of Arctic amplification: A research synthesis. *Global and Planetary Change*, *77*, 85–96.
Serreze, M. C., & Francis, J. A. (2006). The Arctic amplification debate. *Climatic Change*, *76*, 241–264.
Simmonds, I. (2015). Comparing and contrasting the behaviour of Arctic and Antarctic sea ice over the 35 year period 1979–2013. *Annals of Glaciology*, *56*, 18–28.
Simmons, A., Uppala, S., Dee, D., & Kobayashi, S. (2007). ERA-Interim: New ECMWF reanalysis products from 1989 onwards. *ECMWF Newsletter*, *110*, 25–35.
Sprenger, M., & Wernli, H. (2015). The LAGRANTO Lagrangian analysis tool—Version 2.0. *Geoscientific Model Development*, *8*, 2569–2586.
Stocker, T. F., Qin, D., Plattner, G.-K., Tignor, M., Allen, S. K., Boschung, J., … Midgley, P. M. (2013). IPCC 2013, *Climate change 2013: The physical science basis. Contribution of Working Group I to the Fifth Assessment Report of the Intergovernmental Panel on Climate Change* (pp. 1535). Cambridge, UK: Cambridge University Press.
Stroeve, J., Holland, M. M., Meier, W., Scambos, T., & Serreze, M. (2007). Arctic sea ice decline: Faster than forecast. *Geophysical Research Letters*, *34*, L09501. https://doi.org/10.1029/2007GL029703
The Norwegian Meteorological Institute (2016). Detailed weather statistics for Longyearbyen (Svalbard). Retrieved from http://www.yr.no/place/Norway/Svalbard/Longyearbyen/detailed_statistics.html
Tjernström, M., Shupe, M. D., Brooks, I. M., Persson, P. O. G., Prytherch, J., Salisbury, D. J., … Wolfe, D. (2015). Warm-air advection, air mass transformation and fog causes rapid ice melt. *Geophysical Research Letters*, *42*, 5594–5602. http://doi.org/10.1002/2015GL064373
Wernli, H., & Davies, H. C. (1997). A Lagrangian-based analysis of extratropical cyclones. I: The method and some applications. *Quarterly Journal of the Royal Meteorological Society*, *123*, 467–489.
Wernli, H., & Papritz, L. (2017). Role of polar anticyclones and midlatitude cyclones for Arctic summertime sea ice melting. *Nature Geoscience*, https://doi.org/10.1038/s41561-017-0041-0, in press.
Willett, H. C. (1950). *Temperature trends of the past century*. Paper presented at Centenary Proceedings of the Royal Meteorological Society (pp. 195–206). London.
Winton, M. (2006). Amplified Arctic climate change: What does surface albedo feedback have to do with it? *Geophysical Research Letters*, *33*, L03701. https://doi.org/10.1029/2005GL025244
Woods, C., & Caballero, R. (2016). The role of moist intrusions in winter Arctic warming and sea ice decline. *Journal of Climate*, *29*, 4473–4485.